On-Chip mm-Wave Single Pixel Imager for Biomedical Applications

Mostafa M. Zaky, Islam A. Eshrah, Ahmed N. Mohieldin, Ahmed Eladawy
Electronics and Electrical Communications Department
Faculty of Engineering, Cairo University
Giza, 12613, Egypt
email: mostafa.zaky12@cu.edu.eg, {isattar,anader}@eng.cu.edu.eg,g, aeladawy74@gmail.com

***Abstract*—In this work, a mm-Wave single pixel imager is presented. The proposed design is composed of two on-chip dipole antennas over an Artificial Magnetic Conductor (AMC). The transmitting antenna has more than 2 dBi gain at the broadside direction around 90 GHz and about 18-GHz matching bandwidth. Simulations of the coupling between transmitting (Tx) and receiving (Rx) antennas show an object resolution of $2 \times 2.3\,mm^2$and 0.2 dB per unit increase in the relative permittivity. Full-wave simulations are used to obtain the results.**

***Index Terms*—mm-Wave, on-chip antenna, Artificial Magnetic Conductor, Biomedical Imaging .**

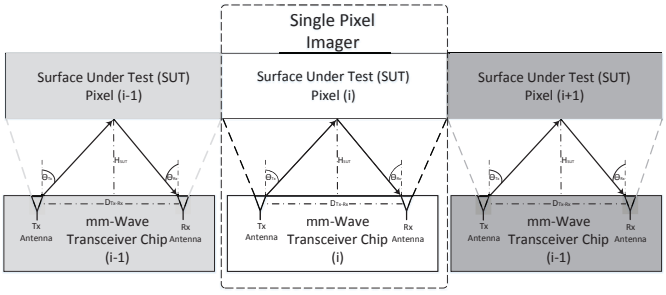

Fig. 1. Single Pixel Imager Array.

I. Introduction

Recently, biomedical imaging has been of a great interest and under dense investigations, especially using microwave techniques. Most of the current medical imaging devices are bulky and costly; consequently they are not available to the consumer directly. Realizing these medical devices using electronic circuits will reduce their cost and increase the early detection probability through the continual monitoring at the patient's side [1]; depending on the fact that the complex permittivity of a tissue can be extracted by subjecting it to Electro-Magnetic (EM) waves [2].

Millimeter wave technology shows a promising performance in medical applications. Millimeter wave transceivers have been used for breast cancer imaging, non-invasive glucose monitoring, and dental caries detection [3]. Another significant advantage at the mm-Wave range is the small wavelengths which makes the antennas easy to integrate on-chip [4].

In order to scan a body, we need to transmit an EM wave and then receive the reflected wave which includes information about the body characteristics as shown in Fig. 1. At mm-Wave range, on-chip antennas could be realized using CMOS technology. A plethora of research has been done on how to realize an on-chip antenna using CMOS or BiCMOS technologies to exploit Moore's law and reduce the device cost [4-9]. However, on-chip antenna design suffers from the high permittivity silicon substrate which makes the main beam of the antenna directed downward to the substrate [5]. Different ways were proposed to alleviate this issue. In [6], a ground sheet is used below the substrate as a reflector. Although, this Perfect Electric Conductor (PEC) could be easily integrated in the PCB holding the chip, the radiation efficiency becomes strongly dependent on the substrate thickness. In addition, due to high coupling to the substrate, surface waves may adversely affect the radiation efficiency and result in non-uniform radiation patterns [7]. Due to the surface waves, the choice of the antenna location, relative to the chip edges becomes very critical. In our case, two on-chip antennas are used (one for Tx and the other for Rx) and it is required to separate them as much as possible to reduce direct coupling. This results in placing each antenna close to one of the chip borders and consequently the main beam directed outside the chip. However, from Fig. 1, the desired radiation pattern for the TX antenna is to have its main lobe toward the Surface Under Test (SUT) (inside the chip) or to be a broadside one.

Instead of using the PEC below the substrate, it can be realized on-chip using the lower metal layer (M1) as in [8], but shortening the distance between antenna and PEC weakens the radiation efficiency. Since the image current of the dipole is in the opposite direction[7].

In order to mitigate the aforementioned issues, another reflector is utilized using High Impedance Surface (HIS). There are several ways to implement HIS for on-chip antennas [9], [10]. H-shaped (dog-bone shaped) layer is used as an AMC to realize low-profile antennas[11], [12]. This has been shown in [10] as an AMC layer under a dipole antenna and also as a radiator, where the dimensions of the unit H-shaped cell were chosen to obtain the magnetic resonance around 90 GHz (close to 94 GHz which is preferred in imaging applications).

 Copyright (C) 2015 IEICE

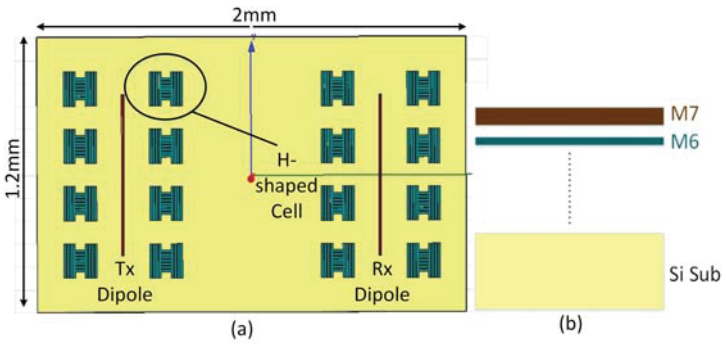

Fig. 2. (a) Top View of the single unit imager chip, showing the Tx/Rx dipole antennas and H-shaped array without the center column. Different colors in (a) corresponds to different metal layers as in (b)

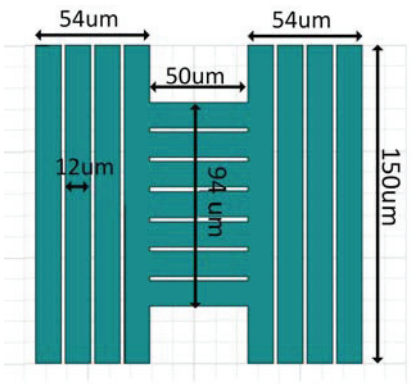

Fig. 3. Modified H-shaped Cell, to satisfy the technology DRC each line is divided into12μm with 2μm spacing

The aim of this work is to design a single unit imager which could be a part of an imager array. The design has been implemented in a low-cost CMOS 65nm technology. The proposed unit imager consists of two antennas, one for Tx and one for Rx, in addition to their RF chain which is beyond the scope of this paper. The proposed on-chip antenna design is presented in section II. The single pixel imager resolution and sensitivity are shown in section III. Finally concluding remarks are drawn in section IV.

II. Proposed On-chip Antenna Design

Two dipole antennas (each of length 0.7 mm) are used for Tx and Rx. For the scenario shown in Fig. 1, the Tx antenna of chip (i) should direct most of its radiated power towards pixel (i) of the SUT. In other words, the Tx antenna radiation pattern should be tilted towards the SUT. These dipoles are located over H-shaped AMC layer. The H-shaped layer has been also used, beside being a HIS, for tilting the main beam of the antenna. The dipoles are located on the top metal layer (M7) and the dog-bone AMC cells are located on M6, as shown in Fig. 2. The central column of the H-shaped AMC cells is removed in order to avoid disturbing the oscillator/other circuits (located in the center of the chip) performance. The total chip size is 2mm×1.2mm.

The H-shaped cell dimensions are 0.4mm×0.25mm as in [10]. The H-shape is divided into strips (12μm width each and 2μm spacing between adjacent lines) to meet the design rules set by the fabrication foundry. The modified H-shape unit cell is shown in Fig.3. A unit cell of the modified H-shape is simulated using using HFSS periodic boundary conditions and the results are shown in Fig. 4. The results show a good agreements with the trends in [10] .

The location of the dipole antenna relative to the surrounding H-shaped cells is varied and its effect on both the return loss (|S11|) and radiation pattern is studied. Initially, the dipole is located at chip center. The corresponding S11 is reported in Fig. 5. In this case the main lobe of the radiation pattern is in the broadside direction as shown in Fig. 5 (red curves). This could be interpreted as the dipole has a complete symmetry from both sides and the AMC layer will act as a

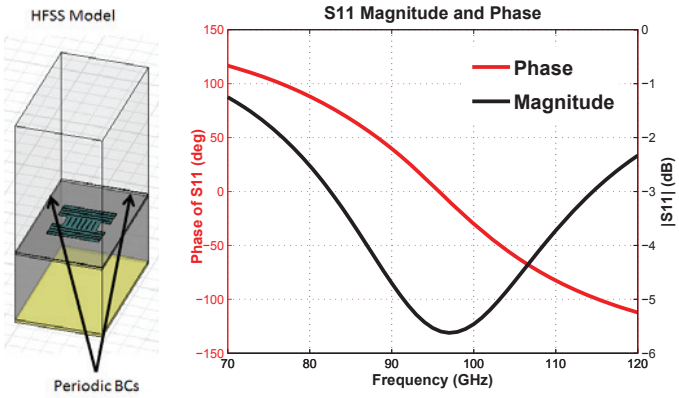

Fig. 4. (a) HFSS Model for the modified H-shaped unit cell, where periodic BCs are used in the side walls and plane wave is incident from the top side. (b) Magnitude and Phase of S11 (de-embedded to the H-shaped cell surface).

very good reflector in this case. But if the dipole antenna is shifted left from the chip center then dipole is surrounded with asymmetric environment and therefore it will be more directive. Fig. 6 shows the gain patterns for both centered dipole , 0.2 mm and 0.6mm shifted dipole from the chip center. It is shown that the 0.6 mm shifted dipole has its main lobe inside the chip with a gain > 4 dBi at the range $10^o < \theta_{Tx} < 70^o$. This can be illustrated as the effective relative permittivity is not equal for the two dipole sides. Although the minimum point of S11 for the 0.6mm shifted dipole is deviated away from 90 GHz, the -10 dB range still covers the frequencies from 82 GHz to 100 GHz as shown in Fig. 5 (blue curve).

With the same analogy, the Rx dipole is then located at 0.6mm right from the center and therefore its radiation pattern is a mirror of the Tx one. Consequently, in Fig. 1, $D_{Tx-Rx} = 1.2mm$ and approximately $H_{SUT} = 2 - 5mm$. Therefore the range of the angles of interest at the Tx is $13^o < \theta_{Tx} < 30^o$. Therefore the chosen locations satisfies the required functions.

After optimizing the locations of Tx and Rx antennas locations, the coupling between them (S21) is simulated to

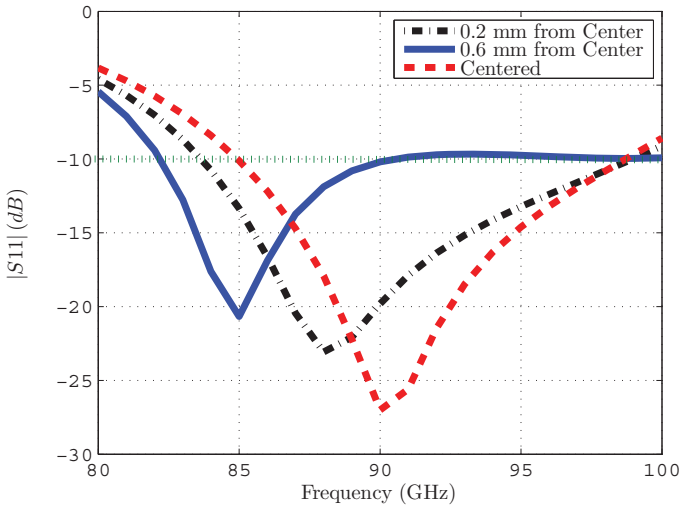

Fig. 5. S11 of dipole antenna at different locations from the center

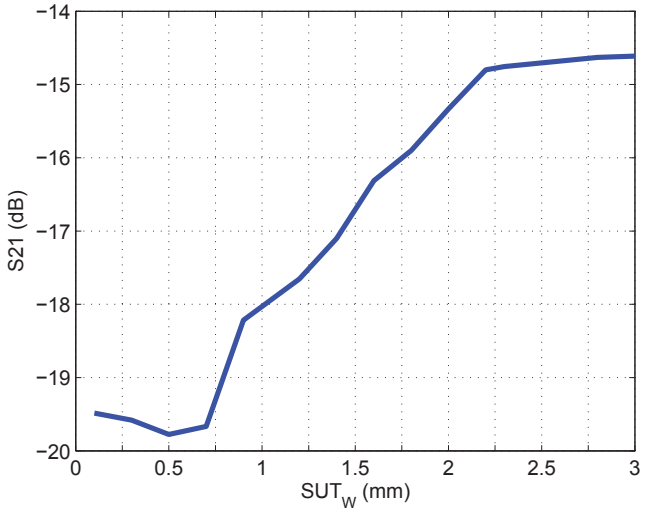

Fig. 7. |S21| variations versus the SUT_W, where H_{SUT} is 2mm, $\epsilon_r = 20$ and frequency = 90GHz.

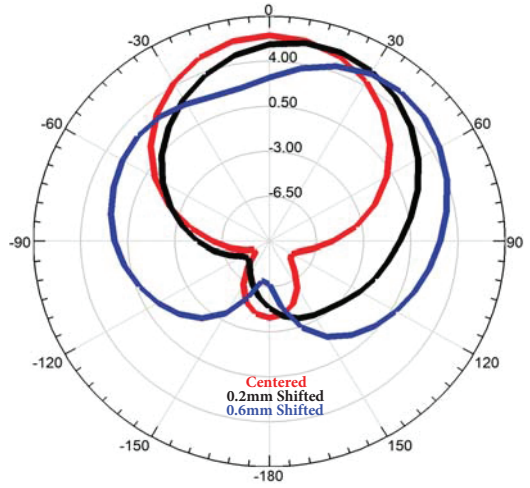

Fig. 6. Gain pattern at 90GHz of dipole antenna at different locations from the center (only the H-plane is shown).

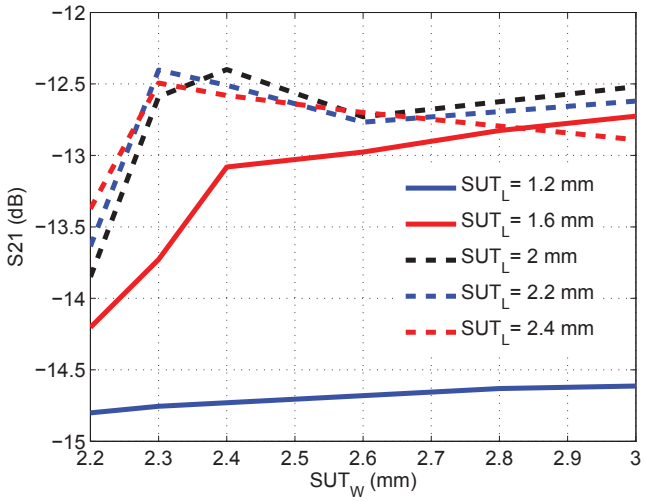

Fig. 8. |S21| variations versus SUT_W for different SUT_L

indicate the SUT size and characteristics.

III. Single Pixel Imager Resolution and Sensitivity

A. Resolution

The SUT is modeled by a box with specific relative permittivity (ϵ_r) and area = $SUT_L \times SUT_W$. In order to get the pixel size, SUT_W and SUT_L of this box are varied and the S21 at 90GHz is simulated and reported in Fig. 7 and Fig. 8 respectively. In Fig. 7, SUT_W is swept from 0.1 to 3 mm while $SUT_L$was fixed to 1.2 mm, H_{SUT} is assumed to be 2mm, and $\epsilon_r = 20$. We can figure out that there is no significant effect on S21 value if the SUT_W is smaller than 0.8mm or larger than 2.2mm. Consequently, the resolution of this single pixel width (SUT_W) is 2.2 mm. Thence, SUT_L is increased from 1.2 to 2.4 mm and S21 at 90 GHz is simulated and plotted versus SUT_W in the range from 2.2 to 3 mm as shown in Fig. 8. We can notice that if SUT_L is larger than 2 mm then S21 is approximately constant with the increase of SUT_L. From Fig. 8, the resolution of single pixel imager is approximately $2\,mm \times 2.3\,mm$ and the other imaging array elements cover next pixels.

B. Sensitivity to Relative Permittivity Change

For a 1.2mm×1.2mm SUT, ϵ_r is varied from 3 to 35 and the effect on |S21| at 90 GHz is reported in Fig. 9. It is shown that |S21| increases with ϵ_r . In other words, as ϵ_r increases the reflected power increases and therefore |S21| increases as well. This may be interpreted as the magnitude of the reflection coefficient is mainly proportional to the difference between refractive indices of air and the scanned surface.

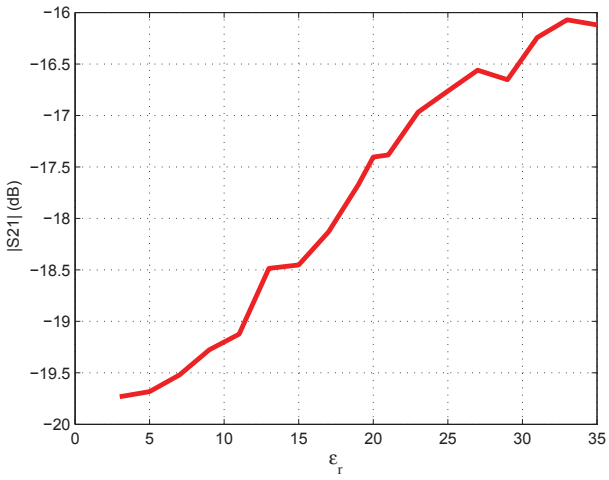

Fig. 9. |S21| versus ϵ_r at 90 GHz.

Approximately, each 5 units increase in ϵ_r results in 1 dB increase in |S21|.

IV. Conclusion

A mm-Wave single pixel imager is presented using two dipole antennas (Tx and Rx) over H-shaped AMC layer. This AMC layer serves two purposes. It is used as a HIS to act as a reflector and suppress the coupling to the substrate as much as possible. It is also used to tilt the radiation pattern towards the SUT. EM simulation results show a pixel resolution of 2mm×2.3mm and antennas peak gain of 4 dBi at 90 GHz.

Acknowledgment

The authors would like to thank Dr. Mohamed Aboudina for his contribution. This work was supported by the Egyptian Information Technology Industry Development Agency (ITIDA) under ITAC program CFP #83.

References

[1] A. Arbabian, S. Callender, S. Kang, B. Afshar, J.-C. Chien, and A. Niknejad, "A 90 GHz Hybrid Switching Pulsed-Transmitter for Medical Imaging," *Solid-State Circuits, IEEE Journal of*, vol. 45, no. 12, pp. 2667–2681, Dec 2010.

[2] F. Artis, T. Chen, T. Chretiennot, J.-J. Fournie, M. Poupot, D. Dubuc, and K. Grenier, "Microwaving Biological Cells: Intracellular Analysis with Microwave Dielectric Spectroscopy," *Microwave Magazine, IEEE*, vol. 16, no. 4, pp. 87–96, May 2015.

[3] F. Topfer and J. Oberhammer, "Millimeter-Wave Tissue Diagnosis: The Most Promising Fields for Medical Applications," *Microwave Magazine, IEEE*, vol. 16, no. 4, pp. 97–113, May 2015.

[4] H. Cheema and A. Shamim, "The last barrier: on-chip antennas," *Microwave Magazine, IEEE*, vol. 14, no. 1, pp. 79–91, Jan 2013.

[5] A. Babakhani, X. Guan, A. Komijani, A. Natarajan, and A. Hajimiri, "A 77-GHz Phased-Array Transceiver With On-Chip Antennas in Silicon: Receiver and Antennas," *Solid-State Circuits, IEEE Journal of*, vol. 41, no. 12, pp. 2795–2806, Dec 2006.

[6] A. Arbabian, S. Callender, S. Kang, M. Rangwala, and A. Niknejad, "A 94 GHz mm-Wave-to-Baseband Pulsed-Radar Transceiver with Applications in Imaging and Gesture Recognition," *Solid-State Circuits, IEEE Journal of*, vol. 48, no. 4, pp. 1055–1071, April 2013.

[7] S. Pan, F. Caster, P. Heydari, and F. Capolino, "A 94-GHz Extremely Thin Metasurface-Based BiCMOS On-Chip Antenna," *Antennas and Propagation, IEEE Transactions on*, vol. 62, no. 9, pp. 4439–4451, Sept 2014.

[8] S. Pan, D. Wang, and F. Capolino, "Novel high efficiency cmos on-chip antenna structures at millimeter waves," in *Antennas and Propagation (APSURSI), 2011 IEEE International Symposium on*, July 2011, pp. 907–910.

[9] D. Sievenpiper, L. Zhang, R. Broas, N. Alexopolous, and E. Yablonovitch, "High-Impedance Electromagnetic Surfaces with a Forbidden Frequency Band," *Microwave Theory and Techniques, IEEE Transactions on*, vol. 47, no. 11, pp. 2059–2074, Nov 1999.

[10] S. Pan, D. Wang, C. Guclu, and F. Capolino, "High impedance layer for CMOS On-chip Antenna at Millimeter Waves," in *Antennas and Propagation (APSURSI), 2011 IEEE International Symposium on*, July 2011, pp. 903–906.

[11] Y. Wu, S.-C. Huang, Y. Chun-Han, W.-Y. Ruan, and H.-R. Chuang, "60-GHz CMOS artificial magnetic conductor on-chip 2x2 monopole - antenna phased array RF receiving system with integrated variable-gain low-noise amplifier and phase shifter," in *Microwave Symposium (IMS), 2014 IEEE MTT-S International*, June 2014, pp. 1–3.

[12] G. Q. Luo, L. Q. Wu, and X. H. Zhang, "An AMC Backed Folded Dipole Slot Antenna Based on CMOS Process," *International Journal of Antennas and Propagation*, vol. 2013, 2013, Hindawi Publishing Corporation, 4 pages.